

Human2Robot: Learning Robot Actions from Paired Human-Robot Videos

Sicheng Xie, Haidong Cao, Zejia Weng, Zhen Xing, Shiwei Shen, Jiaqi Leng,
Xipeng Qiu, Yanwei Fu, Zuxuan Wu, Yu-Gang jiang
Fudan University

Abstract

Distilling knowledge from human demonstrations is a promising way for robots to learn and act. Existing work often overlooks the differences between humans and robots, producing unsatisfactory results. In this paper, we study how perfectly aligned human-robot pairs benefit robot learning. Capitalizing on VR-based teleoperation, we introduce *H&R*, a third-person dataset with 2,600 episodes, each of which captures the fine-grained correspondence between human hand and robot gripper. Inspired by the recent success of diffusion models, we introduce HUMAN2ROBOT, an end-to-end diffusion framework that formulates learning from human demonstration as a generative task. HUMAN2ROBOT fully explores temporal dynamics in human videos to generate robot videos and predict actions at the same time. Through comprehensive evaluations of 4 carefully selected tasks in real-world settings, we demonstrate that HUMAN2ROBOT can not only generate high-quality robot videos but also excels in seen tasks and generalizing to different positions, unseen appearances, novel instances, and even new backgrounds and task types.

1. Introduction

The ability to observe others, whether people or animals, and learn skills to solve new tasks is a key reason humans can handle a wide range of complex challenges. To develop robots capable of assisting with various everyday problems, they must also acquire this skill, particularly the ability to learn directly from humans. This motivates a plethora of work studying how to effectively learn from human demonstrations [4, 5, 38, 53, 56, 60]. However, due to the discrepancies between humans and robots, existing work [38, 60, 71] struggles to transfer learned representations from humans to robots, or simply enforce consistent outputs between humans and robots [4] without considering motion trajectories.

In this paper, we advocate that fine-grained alignment between humans and robots is of great significance. Coarse-grained data provides limited clues for key points and can-

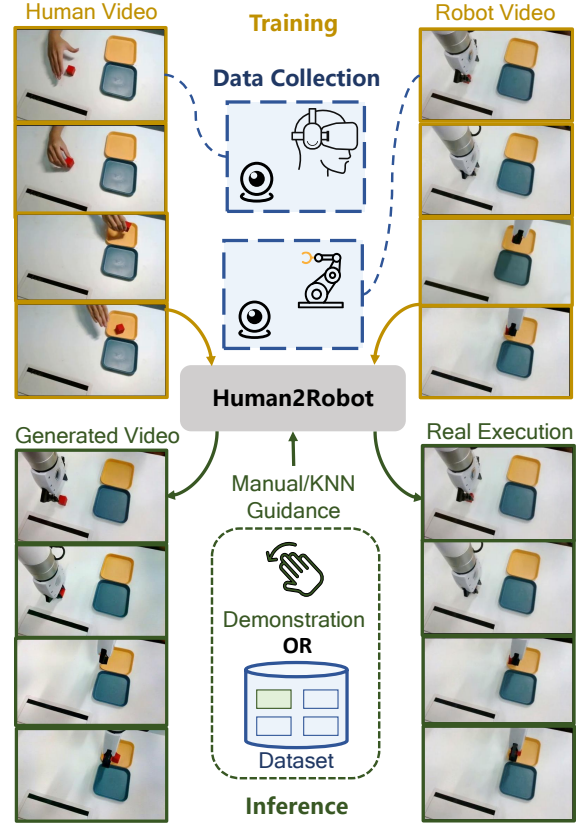


Figure 1. HUMAN2ROBOT: An end-to-end generative framework that simultaneously predicts robotic videos and actions.

not capture detailed information, such as different movement trajectories or grasping positions. While annotating detailed correspondences between humans and robots is feasible [29, 34], it is time-consuming and labor-intensive. Fortunately, virtual reality(VR)-based teleoperation [13, 15, 28, 43] offers a promising way to collect synchronized actions of humans and robots, making it efficient and affordable. This motivates us to build upon VR-based teleoperation for studying paired data that can improve robot learning. In particular, we focus on obtaining perfectly aligned data between humans and robots as a testbed for learning from human demonstrations.

To this end, we introduce a novel data collection pipeline for gathering paired videos of human hands and robotic arms, aligned frame by frame. Unlike previous work that solely collects demonstration data, our method requires minimal additional setup, equipment, or time, making it exceptionally easy to implement and facilitating efficient and consistent data collection. We also introduce the H&R dataset, a third-person dataset featuring perfectly aligned videos of human hands and robotic arms, which includes 8 fundamental tasks and 6 long-horizon tasks, totalling 2,600 episodes. Our goal is to train a model that mimics human actions and performs corresponding tasks based on human demonstrations. This requires the robot to understand how its end effector is aligned with human hands, which is readily available in our dataset, but more importantly, has the ability to act correspondingly. Therefore, the robot needs to predict what actions to take in the future conditioned on human motions as well as historical clues. This is similar in spirit to video generation tasks, that predict future frames (actions) based on various cues [14, 23–25, 37, 41]. As a result, we build upon video generation models to mimic human actions.

In light of this, we introduce HUMAN2ROBOT, an end-to-end generative framework that predicts robotic videos and actions to take simultaneously. In particular, HUMAN2ROBOT is built upon a pretrained Stable Diffusion model, including a spatial UNet for feature extraction, two behavior extractors for motion and position encoding, a spatial-temporal UNet that leverages temporal clues for frame and action prediction. As a result, HUMAN2ROBOT is not only able to generate high-quality robotic videos, which facilitating the expansion of robot-conditioned policies to human-conditioned ones, but can also predict corresponding action trajectory required to perform the task. With carefully designed training strategies, HUMAN2ROBOT not only excels on seen tasks but also generalizes to different positions, unseen appearances, instances and even new backgrounds and task types without additional training. Furthermore, we introduce a KNN-based approach, enabling HUMAN2ROBOT to perform seen tasks even without human demonstrations, providing a flexible and scalable solution to robotic learning from demonstrations.

In summary, our main contributions include:

- We introduce a novel low-cost, low-requirement, high-efficiency, and highly scalable pipeline for collecting perfectly aligned data of humans and robots at the frame level. Additionally, we present H&R, the first dataset featuring perfectly aligned videos of human hands and robotic arms across a variety of tasks, enabling high-fidelity learning from human demonstrations.
- We introduce HUMAN2ROBOT, an end-to-end generative framework built upon a diffusion-based model, capable

of generating robotic videos from human videos while simultaneously predicting the corresponding robotic action trajectories. This approach combines state-of-the-art video generation techniques with multi-task action prediction, facilitating accurate task execution.

- We propose a KNN+HUMAN2ROBOT method, which integrates KNN for task prediction, enabling to perform tasks even without human hand videos as input. This further enhances the scalability and flexibility of the system.
- HUMAN2ROBOT can generate high-quality robotic arm videos, which facilitates the expansion of robot-conditioned policy to human-conditioned policy, while also excelling in four carefully selected tasks, even with variations in positions, appearances, instances, backgrounds and different task types.

2. Related Work

Teleoperation. Researchers have developed various forms of teleoperation approaches for data collection [1–3, 17, 19, 21, 33, 43, 45, 52, 55, 72]. However, these approaches may entail specific device requirements. Recently, VR-based methodologies [15, 28] have attracted considerable attention due to their cost-effectiveness, efficiency and versatility. However, these methods often overlook the importance of the paired visual information. We leverage this perception to capture perfectly aligned videos of humans and robots, which are crucial for robotic imitation.

Learning from Human Videos. Researchers have recently been attempting to leverage existing human-centric video datasets to enhance robot policy learning [10, 34, 51, 54, 71]. Researchers propose to learn representations from human videos to assist in task execution [36, 60, 65]. However, these approaches need substantial prior knowledge and struggle to transfer to robots [4, 5, 38]. Meanwhile, some human-video-conditioned methods [7, 29, 69] have focused on aligning representations across human and robot videos, they are neither efficient nor capable of generalization. In contrast, our approach utilizes paired data and diffusion models to achieve strong generalization capabilities.

Diffusion Models for Video Generation. Due to the remarkable performance of diffusion models in image generation [6, 40, 46, 47, 49], many approaches have explored their potential for video generation [8, 16, 26, 32, 57–59, 64, 67]. Moreover, conditionally controlled video generation [27, 30, 39, 61, 66] has broader and more practical application scenarios. In recent work, several approaches [7, 9, 63] have utilized generative diffusion models to aid policy learning for robots. However, these methods primarily generate videos from a conventional human perspective, often overlooking the distributional differences between human and robotic actions. In contrast, we introduce a novel approach by applying video diffusion mod-

els to robotic scenarios, utilizing a generative model conditioned on human behaviors to guide robotic action outputs.

Diffusion Models for Visual Understanding. The diffusion model not only performs impressively in generative domains but also shows promising applications in visual understanding tasks [18, 35, 50, 70]. Some notable approaches involve using diffusion models for object detection [11], image segmentation [68], and visual representation learning [12, 70]. The approach most similar to ours, GenRec [62] proposes a unified video diffusion model that jointly optimizes video generation and video classification, exhibiting the effectiveness of the diffusion model in video understanding. Our approach is designed for robotic tasks, constructing a human-to-robot video generative model that can simultaneously predict actions for manipulation tasks.

3. H&R Dataset

3.1. Data Collection Pipeline

Our system setup is straightforward, consisting of a Meta Quest 3 VR headset, a 6-DoF xArm robotic arm with a xArm gripper, and two Intel Realsense D435 cameras capturing images of the human hand and robotic arm from the same viewpoint.

The dual-camera setup ensures capturing the synchronized movements of both the human and robotic arms. With the integration of the hardware components, our system aims to achieve a critical objective: *Producing a paired dataset where each data point reflects a seamless synchronization of human hand action and robotic arm response, captured synchronously from identical viewpoints.*

Towards this goal, we build our H&R system focusing on developing software and establishing data collection protocols. We build the control system with OpenTeach [28]. When the user puts on the headset and performs several hand operations, the VR headset sends the coordinates of the hand movements of the user to the robotic arm and achieves synchronized actions.

Achieving this functionality requires addressing issues such as coordinate alignment, precision, and jitter. The details of the implementation are provided in the Supplementary materials B.2.

3.2. Statistics of H&R Dataset

With our designed system and data collection pipeline, we propose our H&R dataset, the first dataset featuring paired human and robotic videos. Human events vary from 8 fundamental tasks and 6 long-horizon tasks. The whole dataset includes 2,600 episodes, and each episode contains frames ranging from 300 to 600. Details can be found in Supplementary materials C.

To the best of our knowledge, the H&R dataset is the first video dataset that ensures perfectly aligned video between

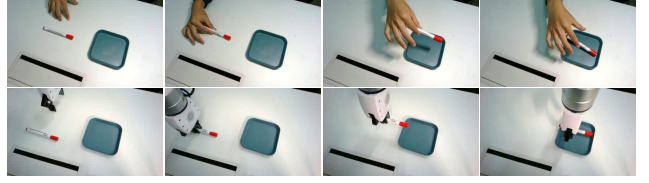


Figure 2. **Data demonstration.** The image above shows a sample from our dataset, recorded simultaneously by two cameras—one for the human and one for the robot—while the user wears a VR headset to perform the operation using our pipeline.

human and robot.

4. HUMAN2ROBOT

Our goal is to develop a model capable of learning from human demonstrations to predict future robot observations and corresponding actions. Formally, we aim to establish a universal policy π that predicts future robot observations $o_{t:t+n}^r$ and action trajectories $a_{t:t+n}$, leveraging inputs from a sequence of hand demonstration videos $o_{t:t+n}^h$, environmental observations o_t^r , and the current proprioception s_t :

$$a_{t:t+n}, o_{t:t+n}^r = \pi(o_{t:t+n}^h, o_t^r, s_t), \quad (1)$$

where n represents the length of the action trajectory we aim to predict. This setting requires the model to not only predict the executed actions but also visually simulate future interactions between the robot arm and objects.

4.1. Architecture

Inspired by the recent success of video diffusion models that are able to predict high-fidelity future frames [20], HUMAN2ROBOT formulates the behavior learning process from human demonstrations as a generative task—generating robot videos and their corresponding actions simultaneously, conditioned on human videos and historical context. Inspired by [27], HUMAN2ROBOT explores a Spatial UNet and a Spatial-Temporal UNet, working collaboratively to learn from humans. In particular, the Spatial UNet extracts features from the robot arm, which is further fed into the Spatial-Temporal UNet for temporal modeling. HUMAN2ROBOT also contains two behavior extractors that estimate position and motion clues using human videos. To achieve action prediction, we use the intermediate features from the Spatial-Temporal UNet to predict the action trajectory via a Policy Head. Figure 3 gives an overview of our pipeline. Below, we introduce the architecture in detail.

Spatial UNet. The Spatial UNet, consisting of 4 upsampling blocks and 4 downsampling blocks, extracts useful clues from the robot arm. In particular, each block, known as the Spatial Layer, leverages self-attention to learn features tailored for robot arms, as well as cross-attention with pre-extracted CLIP embedding to incorporate semantic clues. The weights of the Spatial-UNet are initialized

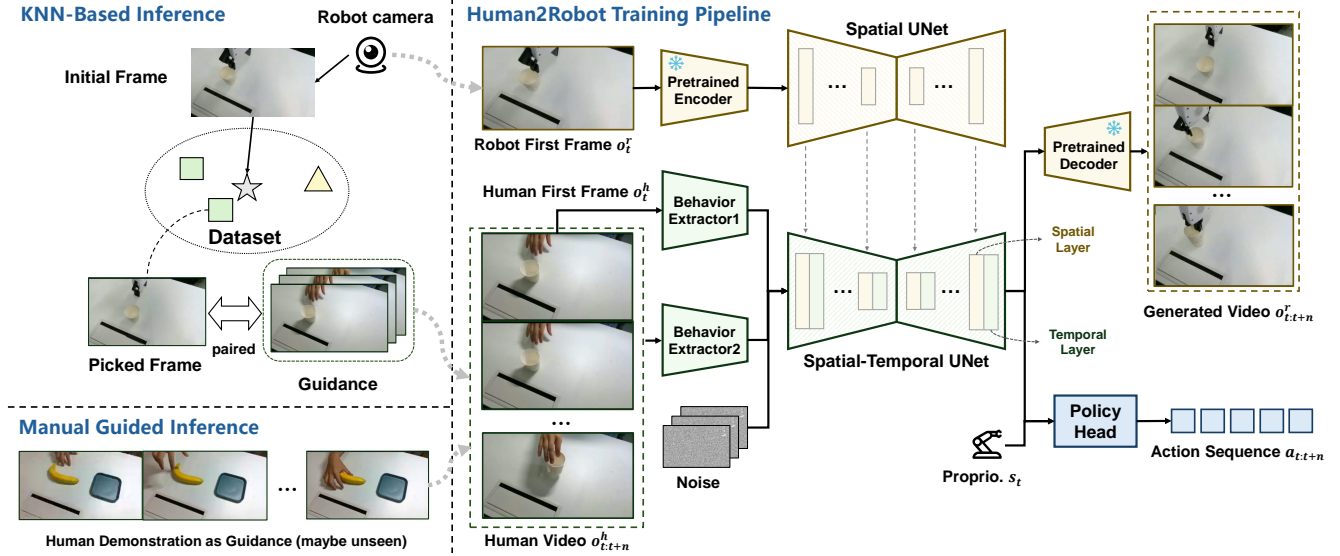


Figure 3. **Architecture overview of HUMAN2ROBOT.** Our approach consists of two training stages. In the first stage, only Behavior Extractors and Spatial Layer in both Spatial UNet and Spatial-Temporal UNet are trainable. In the second stage, we only train Temporal Layer and Policy Head. The Pretrained Encoder and Decoder are frozen all the time. In inference, we have two different modes: the KNN-Based mode can complete seen tasks without hand video, while the Manual Guided mode can complete both seen and unseen tasks. Proprio refers to the proprioception of the robot.

from those of the Stable Diffusion [48] to ease the learning process. The features derived by Spatial-UNet provide a condition for predicting future frames as well as actions.

While Spatial UNet introduces a similar number of parameters as the denoising UNet, it only extracts features once during the entire process, unlike diffusion-based video generation where each frame undergoes denoising multiple times. Therefore, it does not significantly increase computational overhead during inference.

Behavior Extractor. Recall that we aim to learn from human demonstrations, and thus it is important to extract motion and position information from human videos. This is achieved by Behavior Extractor, which contains four convolution layers ($4 \times$ kernels, with a stride of 2). To focus more on the motion trajectories, we employ two independent Behavior Extractors. Behavior Extractor 1 takes the image of the hand corresponding to the robot at the first time step, and Behavior Extractor 2 takes the future image or the entire video of the hand as inputs depending on the training stage, as will be introduced in Section 4.2.

Spatial-Temporal UNet. The Spatial-Temporal UNet aims to predict future frames as well as actions to take simultaneously, requiring the model to learn temporal dynamics. Thus, each block of the Spatial-Temporal UNet (ST-UNet in short) has a Spatial Layer which is the same as the one in Spatial UNet (S-UNet in short), followed by an additional Temporal Layer. More specifically, the ST-UNet takes the features from the behavior extractors and noise latent as inputs. Each Spatial Layer in ST-UNet also concatenates the features of the corresponding layer of the S-UNet, exploring

the robot arm as references for prediction. The Temporal Layer focuses on temporal modeling so as to produce high-fidelity future frames as well as accurate action trajectories.

Policy Head. We aim to generate future frames as well as actions to take within a single unified framework. Drawing from the insights of [62], we propose to divide the UNet mapping function into two distinct components: $F = F_{tail} \cdot F_{head}$. We treat F_{head} as a feature extractor for motion information. This is achieved by passing the intermediate features from UNet and proprioception data s_t to a light-weighted Multilayer Perceptron to predict the actions of the robotic arm.

Pretrained Encoder and Decoder. HUMAN2ROBOT builds upon Stable Diffusion [48], which consists of an encoder and a decoder. The encoder turns images into latent embeddings for fast denoising, and the decoder maps the latents back to images. During training, both the encoder and decoder are kept frozen.

4.2. Training

Our approach consists of two training stages. In the first stage, we focus on image generation by taking the first frame of o_t^r , the first frame of human o_t^h and future frame of human o_{t+i}^h as inputs to predict the future frame of robot o_{t+i}^r . In this stage, we train the S-UNet, the Behavior Extractors, and the ST-UNet without the temporal layers. The spatial layers in both the ST-UNet and S-UNet are instantiated using the powerful open-source Stable Diffusion model (SD) [48], while the Behavior Extractors are initialized with Gaussian weights, except for the final projection layer,

which utilizes zero initialized convolution.

In the second stage, we concentrate the training effort on the temporal layer. In this stage, we take a 30-frame segment of human video $o_{t:t+n}^h$ and the first frame o_t^r of the robot video $o_{t:t+n}^r$ as inputs to predict the future robot observation $o_{t:t+n}^r$ and action $a_{t:t+n}$. The first frame of the robot video is fed into Behavior Extractor 1, while the entire video segment is passed into Behavior Extractor 2, yielding features x_1^t and $x_2^{t:t+n}$, respectively. Then, we replicate x_1^t by n times and add it to $x_2^{t:t+n}$, which is subsequently added to noise latent and fed to our ST-UNet. The weights of the VAE Encoder and Decoder, as well as the CLIP image encoder are frozen all the time. During our training process, we find that dense sampling (30fps) results in jittering in generated videos. Therefore, we reduce the frame rate to one-fourth of the original, namely cutting the number of frames by three-quarters.

Optimization Objectives. We train HUMAN2ROBOT with both generation and action prediction objectives, aiming for the model to achieve high-quality video generation and accurate action prediction simultaneously. The goal of generation for the model is to predict the applied noise, so the objective of the optimization process is:

$$L_G = \mathbb{E}_{z_{ts}, c, \epsilon, ts} (\|\epsilon - \epsilon_\theta(z_{ts}, c, ts)\|_2^2), \quad (2)$$

the parameters of the formula represent the latent state z_{ts} at time step ts , which is obtained from Spatial-Temporal UNet. The conditioning variable c includes the first frame o_t^r of the robot and a human video $o_{t:t+n}^h$. ϵ denotes the added noise, and $\epsilon_\theta(z_{ts}, c, ts)$ represents the model’s predicted noise.

Our action is divided into three components: $a_t^{pos} \in \mathbb{R}^3$ for 3D position, $a_t^{rot} \in \mathbb{R}^6$ for rotation and $a_t^{grip} \in \{0, 1\}$ for gripper state. We use 6D rotation representation proposed in [31, 73] to guarantee continuous representation. We use MSE loss L_p and L_r for position and rotation respectively, and use BCE loss L_g for gripper state.

To balance the generation and action prediction losses, we used a set of balancing weights to control the contribution of each loss to the overall objective.

$$L = L_G + \lambda_p L_p + \lambda_r L_r + \lambda_g L_g, \quad (3)$$

where, λ_p , λ_r and λ_g are the weights of L_p , L_r and L_g respectively.

4.3. Inference

With the aforementioned designs, HUMAN2ROBOT is able to generate high-quality robot videos and perform actions, using observation captured by the camera of the robot and the provided hand video. We further introduce a set of strategies that facilitate more effective task execution by the robot arm, as will be introduced below.

KNN + HUMAN2ROBOT. To avoid the need to explicitly provide human demonstration videos for every prediction, we use a k-nearest neighbors (KNN) approach to identify the most probable task for the current scene and retrieve the human demonstration video corresponding to the closest matching features as the conditioning input to guide the task execution. Specifically, we use DINOv2 [42] and CLIP [44] as feature extractors to capture features from the first frame of each robotic arm video in the training set. During prediction, we select the k closest features based on the current environment, and the episode with the most frequent and closest match is chosen as the conditioning input, which is depicted in the KNN-Based Inference section of Figure 3.

Using KNN significantly simplifies the process for known tasks. However, for tasks involving different objectives within the same setting—such as pick cube task in Figure 4 and Table 2, as well as for unseen tasks such as handwriting, explicit human video guidance is required to accomplish these tasks effectively.

Temporal Addition of Actions. To mitigate trajectory jittering during sequential prediction, inspired by the approach used in ACT [72], we derive the action not from a single prediction but from a weighted average of multiple prediction steps. In particular, we predict a series of actions $a_{t:t+n}$ at time t , which are then combined with the previously predicted actions to compute the aggregated actions $A_{t:t+n}^t$. This represents the set of actions predicted at time t , to be executed from time t to $t+n$, and can be computed as follows:

$$A_{t:t-m+n}^t = (1 - \gamma)A_{t:t-m+n}^{t-m} + \gamma a_{t:t-m+n}, \quad (4)$$

$$A_{t-m+n:t+n}^t = a_{t-m+n:t+n}, \quad (5)$$

where γ is a hyperparameter, with a larger γ indicating a stronger emphasis on the current prediction, and m ($m \leq n$) refers to the length of the action executed after each prediction. Specifically, when $m = n$, the inference degenerates into sequential prediction.

Inference Acceleration. During inference, the diffusion model typically goes through T denoising steps to generate the output. We explore the effectiveness of using features from different denoising steps in Section 5.4, and find that features obtained from the first half of the denoising stages lead to better results. Therefore, to balance speed and quality, we halt the denoising process after obtaining features from the $\frac{T}{4}$ step, directly predict and execute the action, without waiting for the entire denoising process to complete. It is worth noting that if we aim to achieve the fastest possible speed, we can directly use the one-step denoising features for prediction, which allows us to predict the next 30 steps of actions within 0.6 seconds.

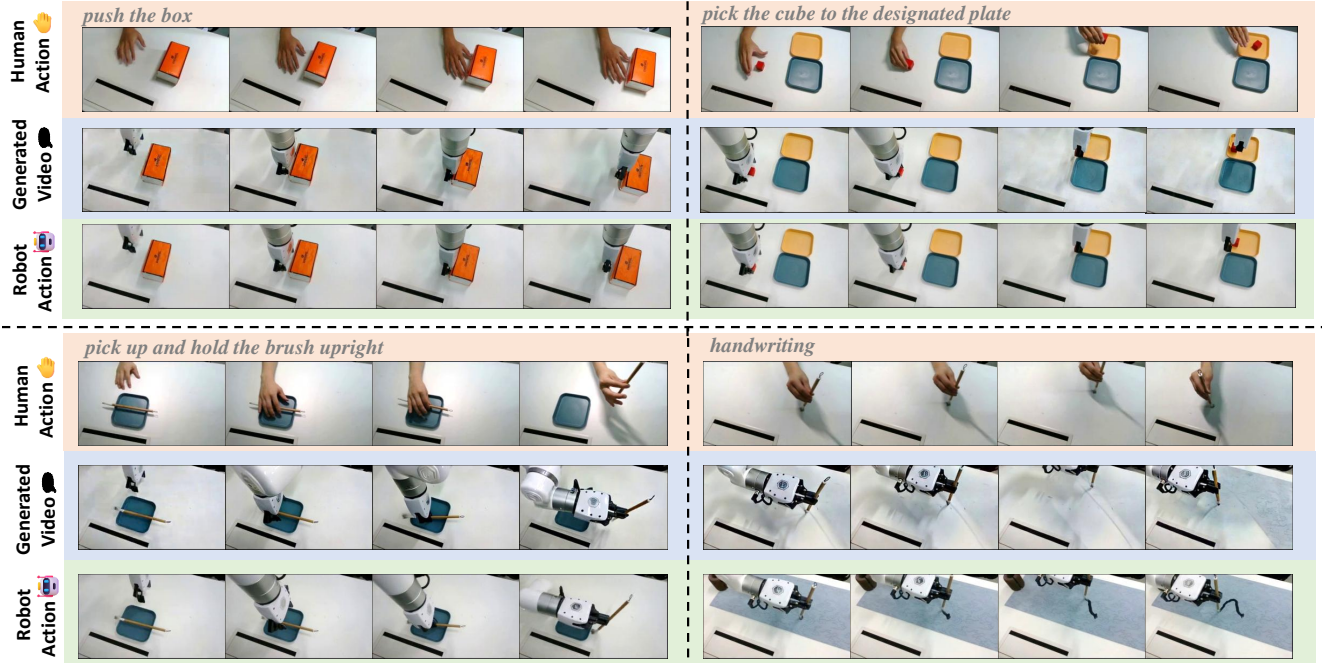


Figure 4. **Qualitative results.** Visualization of generated result and robot action result.

5. Experiments

5.1. Experimental Setups

Task Definition. As visualized in Figure 4, we conduct tests across the following four tasks:

- **Push the box.** Push the box from left to right.
- **Pick the cube to the designated plate.** Pick up the cube and place it on the bottom or top plate depending on the human demonstration.
- **Pick up and hold the brush upright.** Pick up the brush, hold it upright, and get ready to write.
- **Handwriting.** Write the corresponding character depending on the human demonstration.

The four carefully selected tasks above are designed to test the capabilities in multiple aspects: (1) The push box task is to test the accuracy in predicting height, position, and trajectory. (2) The pick cube task requires the model to understand the task objective in the video. (3) The upright task is a challenging fully 6-DOF task. (4) The handwriting task is to test the generalization ability.

Notably, in the handwriting task, the models are evaluated on unseen characters. Since there are countless characters in the world, it is impossible to demonstrate all of them. Therefore, having such a generalization ability is crucial. Thus, this task demands exceptional generalization capabilities, which we have not observed in other models.

Baselines. We compare with the following baselines:

- **RVCD Policy:** We design a robot-video-conditioned policy $\pi(a_t|s_t, v)$, where v refers to the robot video that indicates the task. Specifically, we modify ACT [72] to a

video conditioned policy. Details can be found in Supplementary materials D.2.

- **RVCD Policy w. Generated video:** The framework and weights of this model is the same as RVCD Policy, but the robot video, generated by HUMAN2ROBOT using human demonstration, is provided during inference.
- **XSkill [69]:** XSkill is a human-video-conditioned policy tries to bridge the embodiment gap between human and robot. Details can be found in Supplementary materials D.2.
- **HUMAN2ROBOT w. KNN** HUMAN2ROBOT with our KNN method proposed in Section 4.3, which enables to perform tasks without explicit demonstrations.

The baselines and HUMAN2ROBOT utilize the same H&R dataset for training across all tasks except handwriting. For the handwriting task, the models are trained on handwriting play data [60] (randomly moving data).

5.2. Main results

Effectiveness. As shown in Table 2, HUMAN2ROBOT achieves a high success rate across all tasks. In the pick cube to the designated plate task, half of the test cases require placing the cube on the bottom plate, while the other half require placing it on the top plate. Therefore, a success rate above 50% indicates that the model can correctly follow human demonstrations to perform distinct tasks. However, all baselines perform poorly on this task, consistently placing the cube on the bottom plate regardless of the given demonstration. This proves that only HUMAN2ROBOT can truly understand human demonstration and execute the cor-

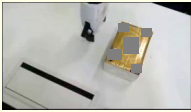









	Appearance		Position		Instance		Background		Bg & Task	
										
Tasks	Push Box		Pick and Place				Upright		Handwriting	
Generalization Type	Apperence		Position		Instance		Background		Bg and Task	
	Brown	Blue	Pos1	Pos2	Pingpong	Banana	Bg1	Bg2	H	R
XSkill [69]	✗	✗	✓	✗	✗	✗	✗	✗	✗	✗
HUMAN2ROBOT	✓	✓	✓	✓	✓	✓	✓	✓	✓	✓

Table 1. **Generalization evaluation.** We evaluate generalization across four different tasks in unseen settings, including variations in appearances, positions, instances, backgrounds, and task targets. The scenes for each task are shown in the figure above. Detailed process can be found in the supplementary materials C. Each setting is evaluated with one trial.

	Push Box	Pick Cube	Upright	Handwriting
<i>RVCD w. Gen</i>	60	30	35	0
<i>RVCD</i>	75	45	40	0
<i>XSkill [69]</i>	70	40	50	0
HUMAN2ROBOT w. KNN	85	40	60	0
HUMAN2ROBOT	95	85	80	90

Table 2. **Main results.** Each task is evaluated with 20 trails.

rect tasks. In addition, all baselines can successfully complete the handwriting task that requires strong generalization exhibiting they have limited generalization capabilities. These results highlight the satisfactory performance and strong generalization capabilities of HUMAN2ROBOT.

We also test our KNN method proposed in Section 4.3, in a setting where no demonstrations are given. The performance of HUMAN2ROBOT w. KNN is shown in Table 2. HUMAN2ROBOT with KNN outperforms all other baselines across all tasks, demonstrating that even without direct demonstrations, HUMAN2ROBOT can still achieve strong performance. However, the KNN method experiences a 10-20% drop in success rate on the push box and upright tasks, which is within an acceptable range. Meanwhile, a significant performance drop is observed in the pick cube to the designated plate task. This is expected, as the KNN method struggles to select the desired demonstration video when faced with the same initial scene. Finally, the KNN method cannot select demonstrations that were not present during training, as these demonstrations are only used during inference. As a result, it fails to accomplish the handwriting task. As a whole, such competitive results demonstrate the high efficiency and accuracy of HUMAN2ROBOT in action prediction with episodes retrieved by KNN.

Quality of Generated Videos. Besides predicting actions, HUMAN2ROBOT can visually simulate future dynamics of

robot movements, requiring precise predictions of the motions of the robot arm and its interactions with objects. The visual quality of the generated video of HUMAN2ROBOT is shown in Figure 4.

However, to evaluate the quality of generated videos, the traditional methods of using video distribution scores presents the following challenges: (1) Since the test set is small, which is common in the robotics domain, typically containing only 5 to 20 test samples, the scores may be unreliable. (2) No existing generation methods are directly applicable to our task.

To this end, we introduce a new visual quality evaluation pipeline: training a RVCD policy as an upper bound and replacing robot-conditioned videos with generated videos during inference. The performance drop serves as a proxy for evaluating visual quality. As shown in Table 2, the performance of RVCD w. Gen achieve a similar score, demonstrating the realism of our video prediction.

5.3. Generalization

Position generalization. HUMAN2ROBOT uses its generative capability to enable the policy to understand human intentions and perform corresponding tasks at different positions. As shown in Table 1, HUMAN2ROBOT achieves better results in different testing positions.

Appearance generalization. Appearance generalization is crucial for the model’s robustness. Since HUMAN2ROBOT is based on Stable Diffusion [48], which contains a vast amount of prior knowledge, it naturally inherits strong generalization capabilities in terms of appearance without any data augmentation. As shown in the Table 1, HUMAN2ROBOT demonstrates excellent generalization across different colors, which are unseen during training.

Instance generalization. Instance generalization requires the ability to generalize across objects of different sizes and shapes, making it even more critical than appearance generalization. As illustrated in the Table 1, thanks to the generative capability of diffusion models, HUMAN2ROBOT achieves strong performance across various objects. HUMAN2ROBOT successfully completes tasks on unseen instances, demonstrating its powerful generalization ability.

Background generalization. Although the training data primarily consists of white backgrounds, as shown in the Figure 4, we find that HUMAN2ROBOT maintains stable performance even when the background color changes or the scene becomes cluttered. As presented in the Table 1, HUMAN2ROBOT successfully completes tasks across different background, demonstrating its strong capability.

Task generalization. We train the model on play data, which involves moving randomly on the table rather than writing any specific character, and then evaluate its one-shot task execution ability given human handwriting prompts of never-before-seen character. To keep the scene clean during data collection, no actual handwriting was performed, resulting in blank backgrounds in the training data, which differ from those in the evaluation phase. Consequently, the handwriting task simultaneously challenges the generalization ability of models in both scene adaptation and task execution. The satisfying results shown in the Table 1 demonstrate the effectiveness and generalization capability of HUMAN2ROBOT in task transfer.

5.4. Discussion

The Choice of Upsampling Layers for Feature Extraction. As shown in Table 3, we examine the impact of extracting features from different UNet upsample layers for action prediction. Using the 2nd up-sampling block (Up Index 2) achieves a 90% success rate on seen tasks, while the 1st up-sampling block (Up Index 1) reaches a 95% success rate on unseen tasks. The results indicate that the choice of upsampling layer has minimal effect on outcomes.

<i>Up Index</i>	Seen Task	Unseen Task
1	85	95
2	90	80
3	80	70

Table 3. Results of different up-sampling blocks.

Studying the Choice of Denoising Step. As shown in Tab 4, During inference, we fix the upsampling layer to extract features from different denoising steps. We find that, due to the MLP being trained with random noise, features from just one denoising step already allow the model to perform well, achieving 80% accuracy on seen tasks and 90% on unseen tasks, with an inference time of 0.6 seconds for 30 step trajectory prediction. Features after 7 denoising

steps (1/4 of the total steps) yield the highest success rate. However, the results are worse at 15 (1/2 total steps) and 22 (3/4 total steps), possibly due to the following reason: the features in the early denoising stages, such as the 1st and 7th denoising stage shown in Figure 5, already capture sufficient spatial information to complete the tasks. However, in later denoising stages, the model focuses more on reconstructing detailed visual information, which increases action variance, making the movements jerky of the robot and ultimately reducing the success rate.

<i>Denoising Step</i>	Seen Task	Unseen Task	Times(s)
1	80	90	0.6
7	85	95	3.2
15	80	80	6.5
22	70	80	9.3

Table 4. Results of different denoising steps.

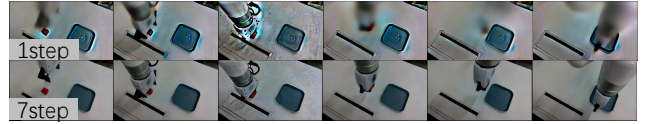


Figure 5. Visual result of 1 and 7 step DDIM.

The Effect of Data Scale. After achieving strong image generation capabilities after the first training stage using the whole dataset, we train the model using different data scales in the second stage to assess its performance across varying amounts of data. As shown in Table 5, we conduct tests across various data scales and discover that even a small amount of data can lead to promising results on previously encountered tasks. For instance, using just 5% of the data(116 episodes) is sufficient to achieve a 70% success rate on seen tasks. The success rate on unseen tasks increases significantly as the amount of data increases.

<i>Data Scale</i>	Seen Task	Unseen Task
0.05	70	30
0.1	70	40
0.2	80	60
1	85	80

Table 5. Results of different data scales.

6. Conclusion

In this paper, we introduced a data collection pipeline for perfectly paired human-robot data and used it to create the H&R dataset. Then we presented HUMAN2ROBOT, a novel end-to-end diffusion framework that simultaneously predicted robot video and actions given a hand video. Next, we leveraged a KNN method to perform tasks without explicitly requiring human hand videos as input. HUMAN2ROBOT not only achieved outstanding performance

on four carefully selected tasks but also demonstrated its capabilities in five generalization ability tests.

A. System Setup Details

The H&R system is equipped with state-of-the-art technology specifically chosen to facilitate seamless and precise interactions between human operators and robotic mechanisms, including a Meta Quest 3 VR headset, a 7-DoF xArm robotic arm, and two Intel Realsense D435 cameras as shown in Figure 7a 7b.

The Meta Quest 3 VR headset is selected for its advanced gesture recognition capability and affordable cost. This gesture recognition capability is integral to our data collection pipeline, providing an efficient and user-friendly way to enhance the natural interaction between human operators and the robotic system. The Xarm robotic arm, which features seven degrees of freedom, provides the flexibility and precision required for complex and varied tasks. This arm is integral to replicating human hand movements accurately, ensuring that the physical actions translated through the VR system are executed precisely by the robotic counterpart. Visual data collection is handled by two Intel Realsense D435 cameras strategically positioned to monitor both human and robot actions. These cameras operate at a resolution of 240×424 pixels, capturing images at 30Hz. The dual-camera setup captures the synchronized movements of both the human and robotic arms. With the integration of the hardware components, our system aims to achieve a critical objective:

Producing a paired dataset where each data point reflects a seamless synchronization of human hand action and robotic arm response, captured synchronously from identical viewpoints.

Toward this goal, we build our H&R system to develop software and establish data collection protocols. We build the control system with OpenTeach [28], connecting different hardware components to enable the operator to perform manual tasks and simultaneously monitor the robotic arm’s actions through the VR headset display. Specifically, we set up two similar environments for human operation and robotic arm operation respectively, as shown in Figure 7, and one camera is placed in each operating space. When the user wears the VR headset and performs hand movements, the headset transmits the coordinates of these movements to the backend, where they are retargeted to control the robotic arm, enabling synchronized actions. Section B illustrates more details about the retargeting process. Here, one of the biggest challenges lies in the inconsistency of the scale and the orientation between the two coordinate systems. In the following, we mainly illustrate our implementation for

achieving the coordinate alignment.

B. Data Collection Details

While collecting data, the operating spaces are shown in Figure 7. During the preparation phase, we will record the positional information of four points within the robot’s operating space: three anchor points and the initial position of the robotic arm. The starting position of the robotic arm is recorded and detailed anchor configurations are provided in Section B.1. Operators are required to wear headsets to perform operations throughout the data collection process. The robotic arm will not follow the hand’s movements until the operator sets three anchor points in their workspace by putting hand on each anchor for a brief period. Our program utilizes six anchor points—three for the human and three for the robot—to align the coordinate systems of both sides, as detailed in Section B.1. Since the coordinate system initiated by the headset may vary slightly each time, it is necessary to make a few adjustments to the positions of objects in the environment before starting the actual data collection. During the data collection process, we will use the right hand for demonstration, while the left hand will control the start and end of recording by pressing the keyboard.

B.1. Coordinate System Alignment

In this section, we provide a detailed explanation of how we align the position and rotation of the coordinate systems for the VR headset and the robotic arm.

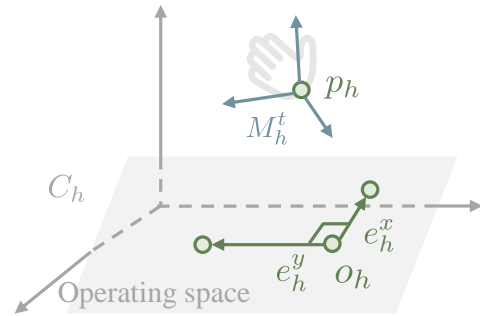


Figure 6. VR headset Coordinate System.

Position alignment. We utilized the introduced anchor points to align the coordinate systems. As illustrated in Figure 6, we select three anchors within the operating space and derive two mutually perpendicular vectors, e_h^x and e_h^y for the human side, and e_r^x and e_r^y for the robot side. These are accompanied by the coordinates of the bottom-right anchor point, o_h and o_r , and are subject to the following constraints in the real world, $|e_h^x|_w = |e_r^x|_w$, $|e_h^y|_w = |e_r^y|_w$ and $e_h^x \cdot e_h^y = e_r^x \cdot e_r^y = 0$, where $|\cdot|_w$ indicates the real-world distance. From these vectors, we calculate the unit vectors e_h^z and e_r^z , which are perpendicular to e_h^x and e_h^y respectively.

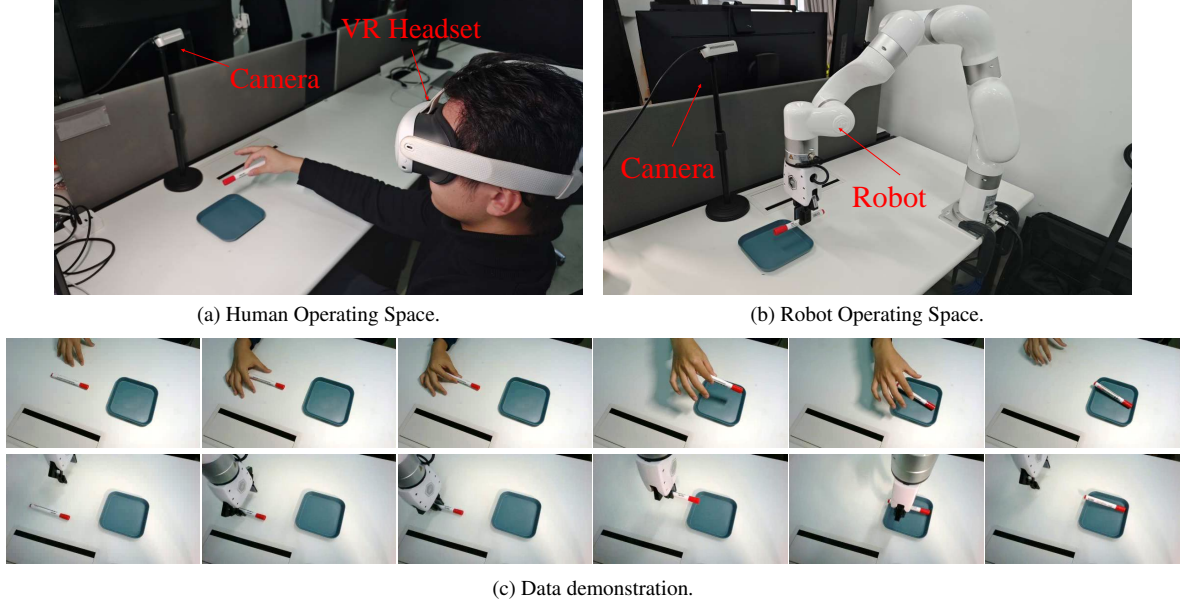


Figure 7. The operating spaces of human and robot

Then, given any hand coordinate p_h , the corresponding robotic arm coordinate p_r can be computed as:

$$p_r = o_r + \mu_x e_r^x + \mu_y e_r^y + \eta \mu_z e_r^z, \quad (6)$$

where η is a hyperparameter that represents the scaling factor of motion amplitude along the z-axis. The value of μ can be computed as follows:

$$\mu_i = \frac{e_h^i \cdot (p_h - o_h)}{|e_h^i|^2}, i \in \{x, y, z\}. \quad (7)$$

Rotation alignment. After aligning the positions, additional alignment is necessary for the orientations. Our goal is to ensure that the relative rotations of the human hand and the robotic arm, relative to their initial states, remain consistent.

To synchronize the rotation of the robotic arm with the human hand, we establish a 3D coordinate system similar to the approach taken by OpenTeach[28]. This coordinate system enables us to compute the rotation matrix M_h^t for the human hand at time t . Additionally, we derive the rotation matrix M_r^t for the robotic arm at the same time t , using the robot's state parameters such as pitch, yaw, and roll. The rotation matrix M_h^t and M_r^t at the time t can be expressed in terms of the rotation matrices M_h^0 and M_r^0 at time $t = 0$ as:

$$M_h^t = M_h^0 R_h^t, \quad (8)$$

$$M_r^t = M_r^0 R_r^t, \quad (9)$$

where R_h^t and R_r^t represent the rotation relative to the coordinate system M_h^0 and M_r^0 respectively. Recall that our

goal is to ensure the relative rotations are the same, which allows us to derive the following equation:

$$R_r^t = P^{-1} R_h^t P, \quad (10)$$

where P is the transformation matrix defined from the basis of the coordinate system M_r^0 to that of M_h^0 .

Organize Equation 8, 9, and 10, and the target rotation matrix of the robotic arm can be calculated as follows:

$$M_r^i = M_r^0 P^{-1} (M_h^0)^{-1} M_h^i P, \quad (11)$$

B.2. System stability

Accuracy. There are two main factors affecting control accuracy: one is the precision of the data source, i.e., the accuracy of hand gesture recognition, and the other is the accuracy loss caused by mapping hand movements to the robotic arm. Our gesture recognition data comes from the Meta Quest 3, and we found that under sufficient lighting conditions, it provides highly accurate hand tracking.

A traditional mapping approach is to map the wrist position to the end-effector position of robot. However, this creates a topological inconsistency, leading to accuracy errors. A more topologically consistent approach is to map the midpoint between the thumb and index fingertip. While this method preserves structural consistency, it introduces jitter due to the differing speeds of the thumb and index finger when grasping objects. Thus, we track the Metacarpophalangeal Joint (MCP) of the index finger, ensuring both the prevention of jitter and the maintenance of accuracy.

Jitter Handling. We set the control mode to serial, making the system's sensitivity depend on execution speed. By

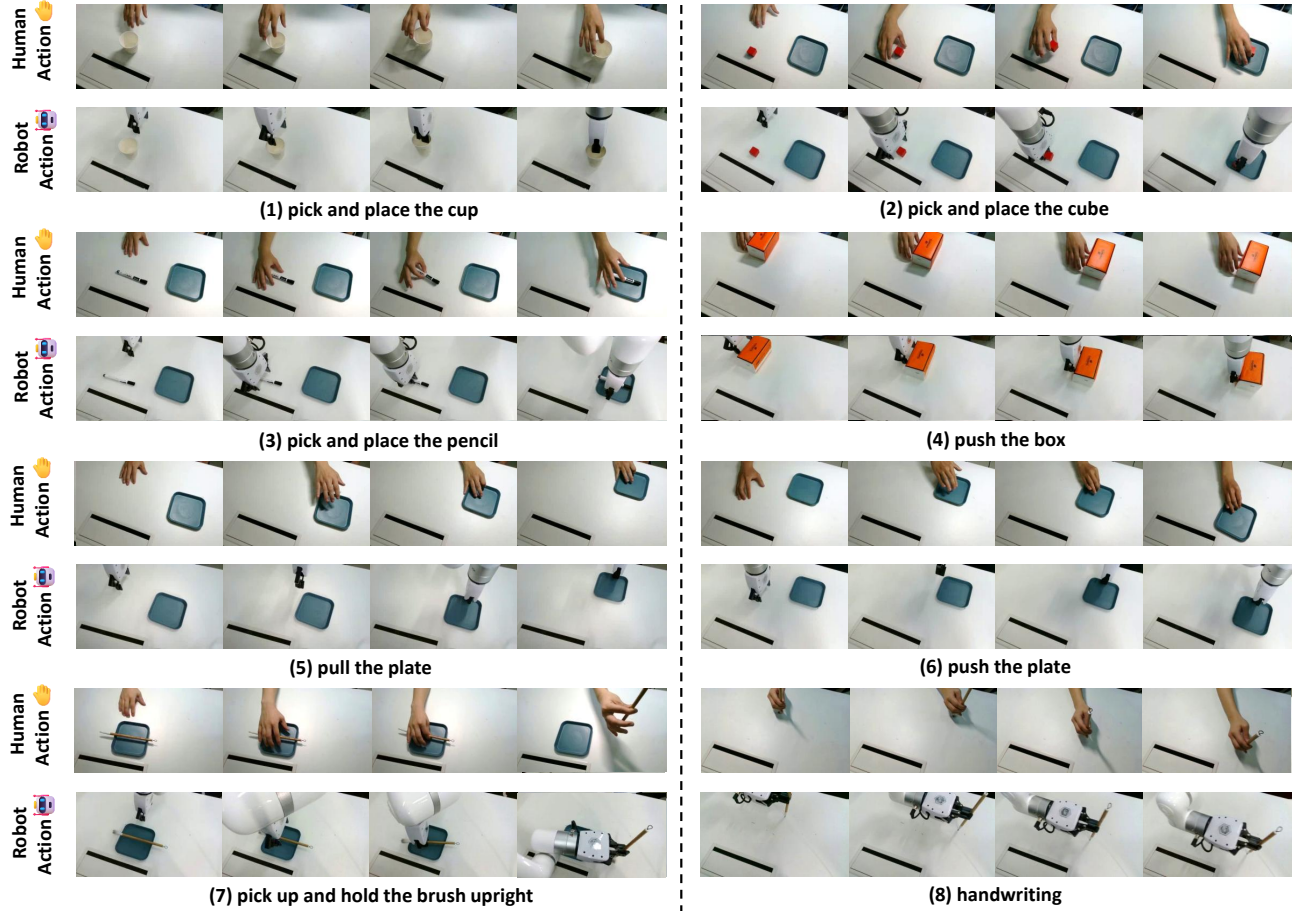


Figure 8. Overview of the dataset for base tasks.

allowing 100–300ms latency, we trade speed for stability, reducing jitter and ensuring smoother motion.

C. H&R Details

C.1. Task Details

Our H&R dataset contains 8 base tasks and 6 long-horizon tasks. The definition of our tasks in our dataset is listed below.

Base tasks. The visual representations of the tasks are shown in Figure 8.

- Pick and place the cup: The cup can initially be placed anywhere on the table. The goal of this task is to pick up the cup and place it in another location.
- Pick and place the cube: The cube comes in two colors (red and green), and it can initially be placed within a designated area. The goal of this task is to pick up the cube and place it on a plate.
- Pick and place pencil: The pencil comes in two colors (red and black), the goal is to pick up the pencil and place it on a plate.
- Push the box: The box comes in two colors (red and

green), and its initial position of it is random. The goal is to push the box from left to right

- Pull the plate: The goal is to pull the plate from bottom to top.
- Push the plate: The goal is to push the plate from top to bottom.
- Pick up and hold the brush upright: The goal is to pick up the brush and upright it.
- Handwriting: Play data, write aimlessly on a blank desk.

Long-Horizon tasks. These tasks are a combination of the base tasks.

- Pick both cubes: There are two red cubes on the table, and the goal is to pick up each cube individually and place them onto the plate.
- Pick the designated cube: There is a red cube and a green cube on the table, and the goal is to pick up one of the cubes onto the plate.
- Pick to the designated plate: There is a red cube and two plates on the table, and the goal is to pick up the cubes onto one of the plates.
- Pick the cube and pull the plate: The combination of pinch a cube and pull the plate. The goal is to first pick



Figure 9. **Visualization of generalization evaluation process.** To accelerate inference, we skip the video generation process when performing the handwriting task.

the cube onto the plate and pull the plate.

- Pull the plate and pick the cube: The combination of pull the plate and pinch a cube. After pulling the plate, the cube should be placed in the plate’s new position.
- Return to the initial position: Complete the base tasks and return to the initial position.

C.2. Episode Details

H&R consists of 2,600 episodes, each containing the following information, adhering to the RT-X standards:

- a paired human hand and robotic arm video containing frames between 200 and 600, with variations depending on the task.
- state of the robotic arm at each timestamp, including position and rotation.
- joint of the robotic arm velocity at each timestamp.
- transform matrix of the human hand, including position and rotation.

- position of each key point of the human hand.
- action of the robotic arm retargeted based on human hand data.
- timestamp.

D. Experimental Details

D.1. Experimental Details

Implementation Details. To demonstrate the effectiveness of our approach, we train our model on H&R. We used 4 NVIDIA A100 GPUs for training in the first stage and 8 4090 GPUs for the second stage. In the first training stage, we use the native image size of 424×240 and conduct training for 15,000 steps and set the total batch size as 128. In the second training stage, the temporal layer and policy header are trained for 50,000 steps using 30-frame video sequences and the total batch size is 8. The learning rates of the two stages are set to 1e-5, and the weights of each objective are

set to $\lambda_p = \lambda_r = \lambda_g = 1$. During inference, we utilize a DDIM sampler for 30 denoising steps and extract features from the first upsample layer and the 7th denoising step for action prediction. The smoothing parameter γ is set to 0.5.

D.2. Baseline Details

RVCD Policy. Here we talk about how we add conditions to ACT [72] in detail. We input the observation information of the robotic arm into the encoder. Then, we add the features of the next n frames of the human hand as a condition to the position embedding and input them into the decoder. Specifically, similar to the method used for processing the original robot images, we input human images into ResNet18 [22] and obtain a feature map of size 300x512. We then pass it through a shared MLP to obtain a feature of size 512, which is added to the position embedding and fed into the Transformer decoder. Both the ResNet18 [22] and MLP are trainable.

XSkill. We replicated xSkill in a real-world setting, where the authors did not fully open-source the code. As a result, we completed the remaining code based on the code from the simulation environment. During the skill discovery and labeled dataset phases, we used the default settings, except for adjusting the num frames parameter of the frame sampler from 100 to 50 to reduce GPU memory consumption. We train this stage for 300 epochs.

In the skill transfer composing phase, we found that performance of XSkill was quite poor. Although the behavior cloning loss decreased significantly, the diffusion policy barely demonstrated any task execution ability after denoising. Since the XSkill [69] paper mentions that any imitation learning policy can be used with the XSkill framework, we replaced the diffusion policy with an action head the same as HUMAN2ROBOT, a simple MLP, for training. During training, we adjusted the prediction horizon to 32, resized the pretraining to 160x120 to maintain consistency with the previous training process, and set the vision feature dimension to 64, in line with the simulation environment. We trained this stage for a total of 2000 epochs until the loss showed no significant changes.

References

- [1] Jorge Aldaco, Travis Armstrong, Robert Baruch, Jeff Bingham, Sanky Chan, Kenneth Draper, Debidatta Dwibedi, Chelsea Finn, Pete Florence, Spencer Goodrich, et al. Aloha 2: An enhanced low-cost hardware for bimanual teleoperation. *arXiv preprint arXiv:2405.02292*, 2024. 2
- [2] Sridhar Pandian Arunachalam, Sneha Silwal, Ben Evans, and Lerrel Pinto. Dexterous imitation made easy: A learning-based framework for efficient dexterous manipulation. *arXiv preprint arXiv:2203.13251*, 2022.
- [3] Sridhar Pandian Arunachalam, Irmak Güzey, Soumith Chintala, and Lerrel Pinto. Holo-dex: Teaching dexterity with immersive mixed reality. In *ICRA*, 2023. 2
- [4] Shikhar Bahl, Abhinav Gupta, and Deepak Pathak. Human-to-robot imitation in the wild. *arXiv preprint arXiv:2207.09450*, 2022. 1, 2
- [5] Shikhar Bahl, Russell Mendonca, Lili Chen, Unnat Jain, and Deepak Pathak. Affordances from human videos as a versatile representation for robotics. In *CVPR*, 2023. 1, 2
- [6] Yogesh Balaji, Seungjun Nah, Xun Huang, Arash Vahdat, Jiaming Song, Karsten Kreis, Miika Aittala, Timo Aila, Samuli Laine, Bryan Catanzaro, et al. ediffi: Text-to-image diffusion models with an ensemble of expert denoisers. *arXiv preprint arXiv:2211.01324*, 2022. 2
- [7] Homanga Bharadhwaj, Debidatta Dwibedi, Abhinav Gupta, Shubham Tulsiani, Carl Doersch, Ted Xiao, Dhruv Shah, Fei Xia, Dorsa Sadigh, and Sean Kirmani. Gen2act: Human video generation in novel scenarios enables generalizable robot manipulation. *arXiv preprint arXiv:2409.16283*, 2024. 2
- [8] Andreas Blattmann, Robin Rombach, Huan Ling, Tim Dockhorn, Seung Wook Kim, Sanja Fidler, and Karsten Kreis. Align your latents: High-resolution video synthesis with latent diffusion models. In *CVPR*, 2023. 2
- [9] Chi-Lam Cheang, Guangzeng Chen, Ya Jing, Tao Kong, Hang Li, Yifeng Li, Yuxiao Liu, Hongtao Wu, Jiafeng Xu, Yichu Yang, et al. Gr-2: A generative video-language-action model with web-scale knowledge for robot manipulation. *arXiv preprint arXiv:2410.06158*, 2024. 2
- [10] Annie S Chen, Suraj Nair, and Chelsea Finn. Learning generalizable robotic reward functions from "in-the-wild" human videos. *RSS*, 2021. 2
- [11] Shoufa Chen, Peize Sun, Yibing Song, and Ping Luo. DiffusionDet: Diffusion model for object detection. In *ICCV*, 2023. 3
- [12] Xinlei Chen, Zhuang Liu, Saining Xie, and Kaiming He. Deconstructing denoising diffusion models for self-supervised learning. *arXiv preprint arXiv:2401.14404*, 2024. 3
- [13] Xuxin Cheng, Jialong Li, Shiqi Yang, Ge Yang, and Xiaolong Wang. Open-television: Teleoperation with immersive active visual feedback. *arXiv preprint arXiv:2407.01512*, 2024. 1
- [14] Prafulla Dhariwal and Alexander Nichol. Diffusion models beat gans on image synthesis. In *NeurIPS*, 2021. 2
- [15] Runyu Ding, Yuzhe Qin, Jiyue Zhu, Chengzhe Jia, Shiqi Yang, Ruihan Yang, Xiaojuan Qi, and Xiaolong Wang. Bunny-visionpro: Real-time bimanual dexterous teleoperation for imitation learning. *arXiv preprint arXiv:2407.03162*, 2024. 1, 2
- [16] Patrick Esser, Johnathan Chiu, Parmida Atighehchian, Jonathan Granskog, and Anastasis Germanidis. Structure and content-guided video synthesis with diffusion models. In *ICCV*, 2023. 2
- [17] Zipeng Fu, Tony Z Zhao, and Chelsea Finn. Mobile aloha: Learning bimanual mobile manipulation with low-cost whole-body teleoperation. *arXiv preprint arXiv:2401.02117*, 2024. 2
- [18] Zigang Geng, Binxin Yang, Tiankai Hang, Chen Li, Shuyang Gu, Ting Zhang, Jianmin Bao, Zheng Zhang, Houqiang Li, Han Hu, et al. InstructDiffusion: A generalist modeling interface for vision tasks. In *CVPR*, 2024. 3

- [19] Abraham George, Alison Bartsch, and Amir Barati Farimani. Openvr: Teleoperation for manipulation. *arXiv preprint arXiv:2305.09765*, 2023. 2
- [20] Yuwei Guo, Ceyuan Yang, Anyi Rao, Zhengyang Liang, Yaohui Wang, Yu Qiao, Maneesh Agrawala, Dahua Lin, and Bo Dai. Animatediff: Animate your personalized text-to-image diffusion models without specific tuning. *arXiv preprint arXiv:2307.04725*, 2023. 3
- [21] Ankur Handa, Karl Van Wyk, Wei Yang, Jacky Liang, Yu-Wei Chao, Qian Wan, Stan Birchfield, Nathan Ratliff, and Dieter Fox. Dexpilot: Vision-based teleoperation of dexterous robotic hand-arm system. In *ICRA*, 2020. 2
- [22] Kaiming He, Xiangyu Zhang, Shaoqing Ren, and Jian Sun. Deep residual learning for image recognition. In *CVPR*, 2016. 13
- [23] Amir Hertz, Ron Mokady, Jay Tenenbaum, Kfir Aberman, Yael Pritch, and Daniel Cohen-Or. Prompt-to-prompt image editing with cross attention control. *arXiv preprint arXiv:2208.01626*, 2022. 2
- [24] Jonathan Ho and Tim Salimans. Classifier-free diffusion guidance. *arXiv preprint arXiv:2207.12598*, 2022.
- [25] Jonathan Ho, Chitwan Saharia, William Chan, David J Fleet, Mohammad Norouzi, and Tim Salimans. Cascaded diffusion models for high fidelity image generation. *JMLR*, 2022. 2
- [26] Jonathan Ho, Tim Salimans, Alexey Gritsenko, William Chan, Mohammad Norouzi, and David J Fleet. Video diffusion models. In *NeurIPS*, 2022. 2
- [27] Li Hu. Animate anyone: Consistent and controllable image-to-video synthesis for character animation. In *CVPR*, 2024. 2, 3
- [28] Aadithya Iyer, Zhuoran Peng, Yinlong Dai, Irmak Guzey, Siddhant Haldar, Soumith Chintala, and Lerrel Pinto. Open teach: A versatile teleoperation system for robotic manipulation. *arXiv preprint arXiv:2403.07870*, 2024. 1, 2, 3, 9, 10
- [29] Vidhi Jain, Maria Attarian, Nikhil J Joshi, Ayzaan Wahid, Danny Driess, Quan Vuong, Pannag R Sanketi, Pierre Sermanet, Stefan Welker, Christine Chan, et al. Vid2robot: End-to-end video-conditioned policy learning with cross-attention transformers. *arXiv preprint arXiv:2403.12943*, 2024. 1, 2
- [30] Johanna Karras, Aleksander Holynski, Ting-Chun Wang, and Ira Kemelmacher-Shlizerman. Dreampose: Fashion video synthesis with stable diffusion. In *ICCV*, 2023. 2
- [31] Tsung-Wei Ke, Nikolaos Gkanatsios, and Katerina Fragkiadaki. 3d diffuser actor: Policy diffusion with 3d scene representations. *arXiv preprint arXiv:2402.10885*, 2024. 5
- [32] Levon Khachatryan, Andranik Movsisyan, Vahram Tadevosyan, Roberto Henschel, Zhangyang Wang, Shant Navasardyan, and Humphrey Shi. Text2video-zero: Text-to-image diffusion models are zero-shot video generators. In *ICCV*, 2023. 2
- [33] Bo Liu, Yifeng Zhu, Chongkai Gao, Yihao Feng, Qiang Liu, Yuke Zhu, and Peter Stone. Libero: Benchmarking knowledge transfer for lifelong robot learning. *arXiv preprint arXiv:2306.03310*, 2023. 2
- [34] YuXuan Liu, Abhishek Gupta, Pieter Abbeel, and Sergey Levine. Imitation from observation: Learning to imitate behaviors from raw video via context translation. In *ICRA*, 2018. 1, 2
- [35] Shuqing Luo, Bowen Qu, and Wei Gao. Learning robust 3d representation from clip via dual denoising. *arXiv preprint arXiv:2407.00905*, 2024. 3
- [36] Arjun Majumdar, Karmesh Yadav, Sergio Arnaud, Jason Ma, Claire Chen, Sneha Silwal, Aryan Jain, Vincent-Pierre Berges, Tingfan Wu, Jay Vakil, et al. Where are we in the search for an artificial visual cortex for embodied intelligence? In *NeurIPS*, 2023. 2
- [37] Chenlin Meng, Yutong He, Yang Song, Jiaming Song, Jiajun Wu, Jun-Yan Zhu, and Stefano Ermon. Sedit: Guided image synthesis and editing with stochastic differential equations. *arXiv preprint arXiv:2108.01073*, 2021. 2
- [38] Suraj Nair, Aravind Rajeswaran, Vikash Kumar, Chelsea Finn, and Abhinav Gupta. R3m: A universal visual representation for robot manipulation. In *CoRL*, 2022. 1, 2
- [39] Haomiao Ni, Changhao Shi, Kai Li, Sharon X Huang, and Martin Renqiang Min. Conditional image-to-video generation with latent flow diffusion models. In *CVPR*, 2023. 2
- [40] Alex Nichol, Prafulla Dhariwal, Aditya Ramesh, Pranav Shyam, Pamela Mishkin, Bob McGrew, Ilya Sutskever, and Mark Chen. Glide: Towards photorealistic image generation and editing with text-guided diffusion models. In *ICML*, 2021. 2
- [41] Alexander Quinn Nichol and Prafulla Dhariwal. Improved denoising diffusion probabilistic models. In *ICML*, 2021. 2
- [42] Maxime Oquab, Timothée Darcet, Théo Moutakanni, Huy Vo, Marc Szafraniec, Vasil Khalidov, Pierre Fernandez, Daniel Haziza, Francisco Massa, Alaaeldin El-Nouby, et al. Dinov2: Learning robust visual features without supervision. *arXiv preprint arXiv:2304.07193*, 2023. 5
- [43] Yuzhe Qin, Wei Yang, Binghao Huang, Karl Van Wyk, Hao Su, Xiaolong Wang, Yu-Wei Chao, and Dieter Fox. Anyteleop: A general vision-based dexterous robot arm-hand teleoperation system. *arXiv preprint arXiv:2307.04577*, 2023. 1, 2
- [44] Alec Radford, Jong Wook Kim, Chris Hallacy, Aditya Ramesh, Gabriel Goh, Sandhini Agarwal, Girish Sastry, Amanda Askell, Pamela Mishkin, Jack Clark, et al. Learning transferable visual models from natural language supervision. In *ICML*, 2021. 5
- [45] Ilija Radosavovic, Tete Xiao, Stephen James, Pieter Abbeel, Jitendra Malik, and Trevor Darrell. Real-world robot learning with masked visual pre-training. In *CoRL*, 2023. 2
- [46] Aditya Ramesh, Prafulla Dhariwal, Alex Nichol, Casey Chu, and Mark Chen. Hierarchical text-conditional image generation with clip latents. *arXiv preprint arXiv:2204.06125*, 2022. 2
- [47] Robin Rombach, Andreas Blattmann, Dominik Lorenz, Patrick Esser, and Björn Ommer. High-resolution image synthesis with latent diffusion models. In *CVPR*, 2022. 2
- [48] Robin Rombach, Andreas Blattmann, Dominik Lorenz, Patrick Esser, and Björn Ommer. High-resolution image synthesis with latent diffusion models. In *CVPR*, 2022. 4, 7

- [49] Chitwan Saharia, William Chan, Saurabh Saxena, Lala Li, Jay Whang, Emily L Denton, Kamyar Ghasemipour, Raphael Gontijo Lopes, Burcu Karagol Ayan, Tim Salimans, et al. Photorealistic text-to-image diffusion models with deep language understanding. In *NeurIPS*, 2022. 2
- [50] Zineb Senane, Lele Cao, Valentin Leonhard Buchner, Yusuke Tashiro, Lei You, Pawel Andrzej Herman, Mats Nordahl, Ruibo Tu, and Vilhelm Von Ehrenheim. Self-supervised learning of time series representation via diffusion process and imputation-interpolation-forecasting mask. In *SIGKDD*, 2024. 3
- [51] Kenneth Shaw, Shikhar Bahl, and Deepak Pathak. Videodex: Learning dexterity from internet videos. *CoRL*, 2022. 2
- [52] Aravind Sivakumar, Kenneth Shaw, and Deepak Pathak. Robotic telekinesis: Learning a robotic hand imitator by watching humans on youtube. *arXiv preprint arXiv:2202.10448*, 2022. 2
- [53] Laura Smith, Nikita Dhawan, Marvin Zhang, Pieter Abbeel, and Sergey Levine. Avid: Learning multi-stage tasks via pixel-level translation of human videos. *arXiv preprint arXiv:1912.04443*, 2019. 1
- [54] Laura Smith, Nikita Dhawan, Marvin Zhang, Pieter Abbeel, and Sergey Levine. Avid: Learning multi-stage tasks via pixel-level translation of human videos. *arXiv preprint arXiv:1912.04443*, 2020. 2
- [55] Shuran Song, Andy Zeng, Johnny Lee, and Thomas Funkhouser. Grasping in the wild: Learning 6dof closed-loop grasping from low-cost demonstrations. *RA-L*, 2020. 2
- [56] Mohan Kumar Srirama, Sudeep Dasari, Shikhar Bahl, and Abhinav Gupta. Hrp: Human affordances for robotic pre-training. *arXiv preprint arXiv:2407.18911*, 2024. 1
- [57] Shuyuan Tu, Qi Dai, Zhi-Qi Cheng, Han Hu, Xintong Han, Zuxuan Wu, and Yu-Gang Jiang. Motioneditor: Editing video motion via content-aware diffusion. In *CVPR*, 2024. 2
- [58] Shuyuan Tu, Qi Dai, Zihao Zhang, Sicheng Xie, Zhi-Qi Cheng, Chong Luo, Xintong Han, Zuxuan Wu, and Yu-Gang Jiang. Motionfollower: Editing video motion via lightweight score-guided diffusion. *arXiv preprint arXiv:2405.20325*, 2024.
- [59] Shuyuan Tu, Zhen Xing, Xintong Han, Zhi-Qi Cheng, Qi Dai, Chong Luo, and Zuxuan Wu. Stableanimator: High-quality identity-preserving human image animation. *arXiv preprint arXiv:2411.17697*, 2024. 2
- [60] Chen Wang, Linxi Fan, Jiankai Sun, Ruohan Zhang, Li Fei-Fei, Danfei Xu, Yuke Zhu, and Anima Anandkumar. Mimicplay: Long-horizon imitation learning by watching human play. *arXiv preprint arXiv:2302.12422*, 2023. 1, 2, 6
- [61] Tan Wang, Linjie Li, Kevin Lin, Chung-Ching Lin, Zhengyuan Yang, Hanwang Zhang, Zicheng Liu, and Lijuan Wang. Disco: Disentangled control for referring human dance generation in real world. *arXiv preprint arXiv:2307.00040*, 2023. 2
- [62] Zejia Weng, Xitong Yang, Zhen Xing, Zuxuan Wu, and Yu-Gang Jiang. Genrec: Unifying video generation and recognition with diffusion models. *arXiv preprint arXiv:2408.15241*, 2024. 3, 4
- [63] Hongtao Wu, Ya Jing, Chilam Cheang, Guangzeng Chen, Jiafeng Xu, Xinghang Li, Minghuan Liu, Hang Li, and Tao Kong. Unleashing large-scale video generative pre-training for visual robot manipulation. *arXiv preprint arXiv:2312.13139*, 2023. 2
- [64] Jay Zhangjie Wu, Yixiao Ge, Xintao Wang, Stan Weixian Lei, Yuchao Gu, Yufei Shi, Wynne Hsu, Ying Shan, Xiaohu Qie, and Mike Zheng Shou. Tune-a-video: One-shot tuning of image diffusion models for text-to-video generation. In *ICCV*, 2023. 2
- [65] Tete Xiao, Ilija Radosavovic, Trevor Darrell, and Jitendra Malik. Masked visual pre-training for motor control. *arXiv preprint arXiv:2203.06173*, 2022. 2
- [66] Zhen Xing, Qi Dai, Zihao Zhang, Hui Zhang, Han Hu, Zuxuan Wu, and Yu-Gang Jiang. Vidiff: Translating videos via multi-modal instructions with diffusion models. *arXiv preprint arXiv:2311.18837*, 2023. 2
- [67] Zhen Xing, Qi Dai, Han Hu, Zuxuan Wu, and Yu-Gang Jiang. Simda: Simple diffusion adapter for efficient video generation. In *CVPR*, 2024. 2
- [68] Jiarui Xu, Sifei Liu, Arash Vahdat, Wonmin Byeon, Xiaolong Wang, and Shalini De Mello. Open-vocabulary panoptic segmentation with text-to-image diffusion models. In *CVPR*, 2023. 3
- [69] Mengda Xu, Zhenjia Xu, Cheng Chi, Manuela Veloso, and Shuran Song. Xskill: Cross embodiment skill discovery. In *CoRL*, 2023. 2, 6, 7, 13
- [70] Sihyun Yu, Sangkyung Kwak, Huiwon Jang, Jongheon Jeong, Jonathan Huang, Jinwoo Shin, and Saining Xie. Representation alignment for generation: Training diffusion transformers is easier than you think. *arXiv preprint arXiv:2410.06940*, 2024. 3
- [71] Jia Zeng, Qingwen Bu, Bangjun Wang, Wenke Xia, Li Chen, Hao Dong, Haoming Song, Dong Wang, Di Hu, Ping Luo, et al. Learning manipulation by predicting interaction. *arXiv preprint arXiv:2406.00439*, 2024. 1, 2
- [72] Tony Z Zhao, Vikash Kumar, Sergey Levine, and Chelsea Finn. Learning fine-grained bimanual manipulation with low-cost hardware. *arXiv preprint arXiv:2304.13705*, 2023. 2, 5, 6, 13
- [73] Yi Zhou, Connelly Barnes, Jingwan Lu, Jimei Yang, and Hao Li. On the continuity of rotation representations in neural networks. In *CVPR*, 2019. 5